

## Comparison of regional carbon flux estimates from CO<sub>2</sub> concentration measurements and remote sensing based footprint integration

Baozhang Chen,<sup>1</sup> Jing M. Chen,<sup>1</sup> Gang Mo,<sup>1</sup> T. Andrew Black,<sup>2</sup> and Douglas E. J. Worthy<sup>3</sup>

Received 1 June 2007; revised 7 September 2007; accepted 7 December 2007; published 7 May 2008.

[1] Quantification of terrestrial CO<sub>2</sub> sources and sinks at regional scales ( $\sim 10^2$ – $10^6$  km<sup>2</sup>) is fundamental to improving our understanding of the terrestrial carbon cycle. Two independent methods to extract the gross primary productivity (GPP) from atmospheric CO<sub>2</sub> concentration measurements were explored and compared in this study. The methods are (1) planetary boundary layer (PBL) carbon budget analysis that allows the estimation of regional GPP at daily time steps from hourly CO<sub>2</sub> concentration measurements and (2) spatially explicit hourly carbon cycle modeling based on remote sensing and then integrating the daily flux field with a concentration footprint function depending on wind and stability. These methods have been applied to a 28-m tower at an old black spruce site near Candle Lake ( $\sim 100$  km NE of Prince Albert: 53.98717°N, 105.11779°W). The estimates of daily GPP by these two approaches agreed well for 2003 (slope = 0.99;  $r^2 = 0.89$ ). In order to test these methods of inferring the regional GPP from mixing ratio measurements, we also compared the estimates of regional GPP with estimates made using eddy covariance (EC) flux measurements, although their respective source areas are different. They had similar seasonal patterns, but the regional estimates were consistently smaller than the local EC flux derived GPP throughout the growing season in 2003. These estimates of annual regional GPP were 649–664 g C m<sup>-2</sup> for 2003 while the EC-derived annual GPP was 819–847 g C m<sup>-2</sup>. The annual difference was about 20–25%. The EC flux footprint of the tower was relatively homogeneous old black spruce while the concentration footprint, which was a few orders of magnitude larger than the flux footprint, covered boreal evergreen and deciduous broadleaf forests, grassland, cropland, and lakes. Nonforested land occupied about 10–50% of the concentration footprint depending on wind direction and speed and was less productive than the black spruce forest. The discrepancies between regional and local GPP estimates reflected the differences in underlying land surfaces represented by the different footprint areas.

**Citation:** Chen, B., J. M. Chen, G. Mo, T. A. Black, and D. E. J. Worthy (2008), Comparison of regional carbon flux estimates from CO<sub>2</sub> concentration measurements and remote sensing based footprint integration, *Global Biogeochem. Cycles*, 22, GB2012, doi:10.1029/2007GB003024.

### 1. Introduction

[2] Ecosystem functioning and its role in the carbon balance are much better understood than before as a result of measuring and analyzing energy and CO<sub>2</sub> fluxes made at sites using the eddy covariance (EC) technique [Baldocchi *et al.*, 2001]. Direct measurements of the terrestrial carbon

flux using these techniques have nearly continuous temporal coverage at an increasing number of sites across continents [Black *et al.*, 1996; Baldocchi *et al.*, 2001]. EC measurements are a rich source of information on temporal variability and environmental controls of CO<sub>2</sub> exchange between the atmosphere and terrestrial ecosystems [Law *et al.*, 2002]. However, EC measurements under Fluxnet programs represent only a very small fraction of the land area, typically less than 1–3 km<sup>2</sup> for each site.

[3] The atmosphere integrates surface fluxes over many temporal and spatial scales and links scalar sources and sinks with concentrations and fluxes. This principle has been successfully used to develop inverse models to estimate annual carbon budgets [Tans *et al.*, 1990; Enting *et al.*, 1995; Fan *et al.*, 1998; Bousquet *et al.*, 1999; Gurney *et al.*, 2002]. However, because of model limitations and paucity

<sup>1</sup>Department of Geography and Program in Planning, University of Toronto, Toronto, Ontario, Canada.

<sup>2</sup>Biometeorology and Soil Physics Group, Faculty of Land and Food Systems, University of British Columbia, Vancouver, British Columbia, Canada.

<sup>3</sup>Air Quality Research Branch, Meteorological Service of Canada, Toronto, Ontario, Canada.

of continental CO<sub>2</sub> observations these studies have yielded carbon fluxes only at coarse resolution, over large spatial regions (i.e., at continental scale [Rodenbeck *et al.*, 2003]).

[4] Progress in carbon balance studies has been achieved at the extreme ends of the spatial-scale spectrum, either large continents (larger than 10<sup>6</sup> km<sup>2</sup>, e.g., global inverse modeling) or small vegetation stands (less than 1–3 km<sup>2</sup>, e.g., EC measurements). Methods to estimate CO<sub>2</sub> sources and sinks at the intermediate scale between continental and local scales are notably lacking. Moreover, the carbon cycle in different regions can vary markedly in response to changing climate [Friedlingstein *et al.*, 2003; Fung *et al.*, 2005]. Reliable estimates of terrestrial CO<sub>2</sub> sources and sinks at intermediate spatial scales (finer than those used in global inversions and larger than local EC flux measurements and roughly defined as the range between 10<sup>2</sup> and 10<sup>6</sup> km<sup>2</sup>) are required to quantitatively account for the large spatial variability in sources and sinks in the near-field of a measurement location [Gerbig *et al.*, 2003], as well as fundamental to improving our understanding of the carbon cycle [Crevoisier *et al.*, 2006].

[5] It is extremely unreliable to upscale stand-level fluxes (i.e., EC measurements) to a region by simple spatial extrapolation and interpolation because of the heterogeneity of the land surface and the nonlinearity inherent in eco-physiological processes [Levy *et al.*, 1999]. It is also challenging to apply atmospheric inversion technique to regional scales for quantifying annual carbon budgets because at such intermediate scales the atmosphere is often poorly constrained [Gloor *et al.*, 1999; Matross *et al.*, 2006]. Moreover, aggregation errors and errors in atmospheric transport, both within the boundary layer and between the boundary layer and free troposphere, can also be formidable obstacles to using these approaches to obtain quantitative estimates of regional carbon fluxes [Lin *et al.*, 2006]. Hence, there is a strong motivation to develop methods to use atmospheric observations to quantify and validate estimates of the carbon balance at these intermediate scales [Lin *et al.*, 2006; Bakwin *et al.*, 2004; Matross *et al.*, 2006; J. M. Chen *et al.*, 2007]. Observations of CO<sub>2</sub> over the continent within the atmospheric boundary layer reflect exchange processes occurring at the surface at a regional scale (10<sup>2</sup>–10<sup>5</sup> km<sup>2</sup>). The flux information contained in CO<sub>2</sub> concentration data represents footprints of up to 10<sup>5</sup> km<sup>2</sup> [Gloor *et al.*, 2001; Lin *et al.*, 2004], which are several orders of magnitude larger than the direct EC flux footprint. This information is therefore much needed in our effort to upscale from site to region. Moreover, the number of CO<sub>2</sub> mixing ratio measurements above the land surface, made by either tower or aircraft, is steadily increasing. Previous efforts to interpret the signal of regional CO<sub>2</sub> exchange making use of tower concentration data have focused on simple one-dimensional planetary boundary layer (PBL) budgets that rely on gradients in CO<sub>2</sub> concentrations between the boundary layer and the free troposphere [Bakwin *et al.*, 2004; Helliker *et al.*, 2004]. These methods are limited to monthly resolution because of the need to smooth and average over several synoptic events [Matross *et al.*, 2006].

[6] The objective of this study is to explore pragmatic and reliable methods to extract the gross primary productivity (GPP) from atmospheric CO<sub>2</sub> concentration measurements on the basis of PBL analysis. Making use of an integrated ecosystem-boundary layer model for simulating ecosystem fluxes and atmospheric diffusion [Chen *et al.*, 2004], we have previously developed a PBL carbon budget methodology that allows the estimation of regional GPP on a daily basis from hourly concentration measurements [B. Chen *et al.*, 2006a, 2006b; J. M. Chen *et al.*, 2007]. As part of this study, we develop another novel methodology to retrieve regional GPP by superimposing the daily concentration footprint on the underlying daily GPP field simulated using a spatially explicit ecosystem model driven by remote sensing inputs. The comparisons of these two independent regional GPP estimates, i.e., one is concentration derived and the other is concentration footprint integrated, have been made for a 28-m tower at an old black spruce site near White Swan Lake, Saskatchewan Canada. From this study, we seek to address the following questions. (1) How well do the estimates of regional GPP from these two independent methods match each other? (2) How well do both methods of deriving regional GPP compare with EC-derived local GPP and what are the reasons? (3) Are these methodologies applicable to retrieving other components of the terrestrial carbon cycle (i.e., net ecosystem productivity  $F_{NEP}$  and ecosystem respiration  $R$ )?

## 2. Materials

### 2.1. Study Site Descriptions

[7] The research site (53.98717°N, 105.11779°W, and 629 m above the sea level) is located approximately 100 km NE of Prince Albert, Saskatchewan, Canada. It is referred to as Southern Old Black Spruce (SOBS) and was established in 1994 as part of the Boreal Ecosystems Atmosphere Study [Sellers *et al.*, 1997]. The EC flux footprint area is dominated by black spruce (*Picea mallana* Mill.) but approximately 15% of the forest consists of deciduous tamarack (*Larix laricina* (DuRoi) K. Koch). The height of the dominant trees is 11 m. The stand density is ~6350 stems per hectare. Its leaf area index (LAI) is about 3.5–3.8 m<sup>2</sup> m<sup>-2</sup>. The last disturbance occurred in 1879. Some Labrador tea (*Ledum groenlandicum* Oeder) is in the understory with a ground cover of mostly feathermoss (*Pleurozium* spp.). This forest is located in a boggy area with many small pockets of standing water. The landscape in the region is predominantly flat, with slight topographical undulations. On the basis of a 40-year climate record made at Waskosia Lake station, the mean annual and growing season (May to September) air temperatures in the region are 1.0°C and 13.4°C, respectively, and the mean annual precipitation is approximately 440 mm, of which 40% falls as snow. This site has an elevated water table and is generally wet. The texture of the mineral soil is sandy clay. The surface organic layer is 20–30-cm thick and carbon storage in this layer is 39.2 kg C m<sup>-2</sup>. Further site details are given by Jarvis *et al.* [1997], Griffiths *et al.* [2003], and Kljun *et al.* [2006].

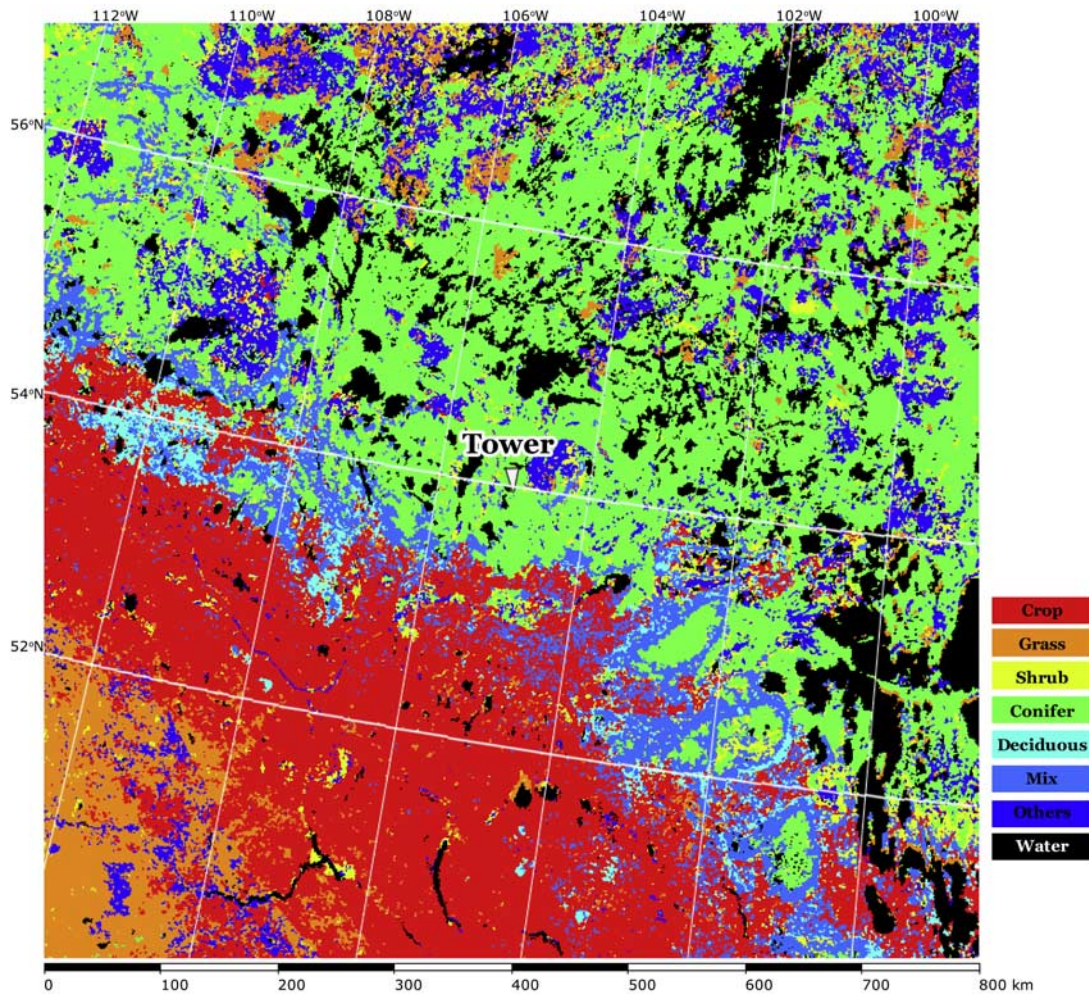


**Figure 1.** Land cover types around the SOBS tower for 2003.

## 2.2. Land Surface Characteristics of the Concentration Footprint

[8] The daily concentration footprint areas of the 28-m tower accumulated for a year could be as large as a circle around the tower up to a 350-km radius (see section 4.2). As shown in Figures 1 and 2, the areas within the footprint are quite heterogeneous. Land cover types (LC) in these areas include conifer forest, deciduous forest, mixed forest, shrub, grass, crop, and nonvegetation type (Figure 1). The dominant LC is conifer forest around the tower within a 100-km radius; while the area to the southeast (>180 km from the tower) is dominated by grass or crop types. The dominant LC types of deciduous and mixed forests are located in the areas to the southeast and southwest from the tower between ~100 and ~180 km. Figure 2 shows a LAI map for August 2003, as an example. LAI varied from 0.5 to  $8 \text{ m}^2 \text{ m}^{-2}$  in the footprint. The LAI for the area surrounding the tower within a 100-km of radius was  $\sim 3.5\text{--}4.5 \text{ m}^2 \text{ m}^{-2}$ .

## 2.3. EC and CO<sub>2</sub> Concentration Measurements

[9] Half-hourly CO<sub>2</sub> and water fluxes and other meteorological variables at this site were measured on a 28-m walk-up scaffold tower using the EC technique. The EC

instruments were mounted at the 25-m height. They included a three-dimensional sonic anemometer-thermometer (model R3; Gill Instruments Limited, United States; Lymington, UK) and a closed-path infrared gas analyzer (model 6262; LI-COR Incorporated, Lincoln, Nebraska, United States) operating in absolute mode for measuring fluctuations in CO<sub>2</sub> and water vapor density. Details about the EC system were given by *Black et al.* [1996], *Arain et al.* [2002], and *Griffis et al.* [2003].

[10] CO<sub>2</sub> concentration was measured at both the 20-m and 28-m heights according to World Meteorological Observation (WMO) Global Atmospheric Watch standards with an accuracy of 0.1 ppm at 15 min intervals. Calibrations using a WMO standard were made at approximately 1-week intervals. Gaps with no valid data at any level were less than 10% year round. Small data gaps of 1 to 2 h were filled by linear interpolation.

## 3. Methods

### 3.1. Model Framework and Assumptions

[11] Meteorological processes such as the entrainment of tropospheric air during boundary layer growth, synoptic-scale subsidence of the troposphere, radiative processes,

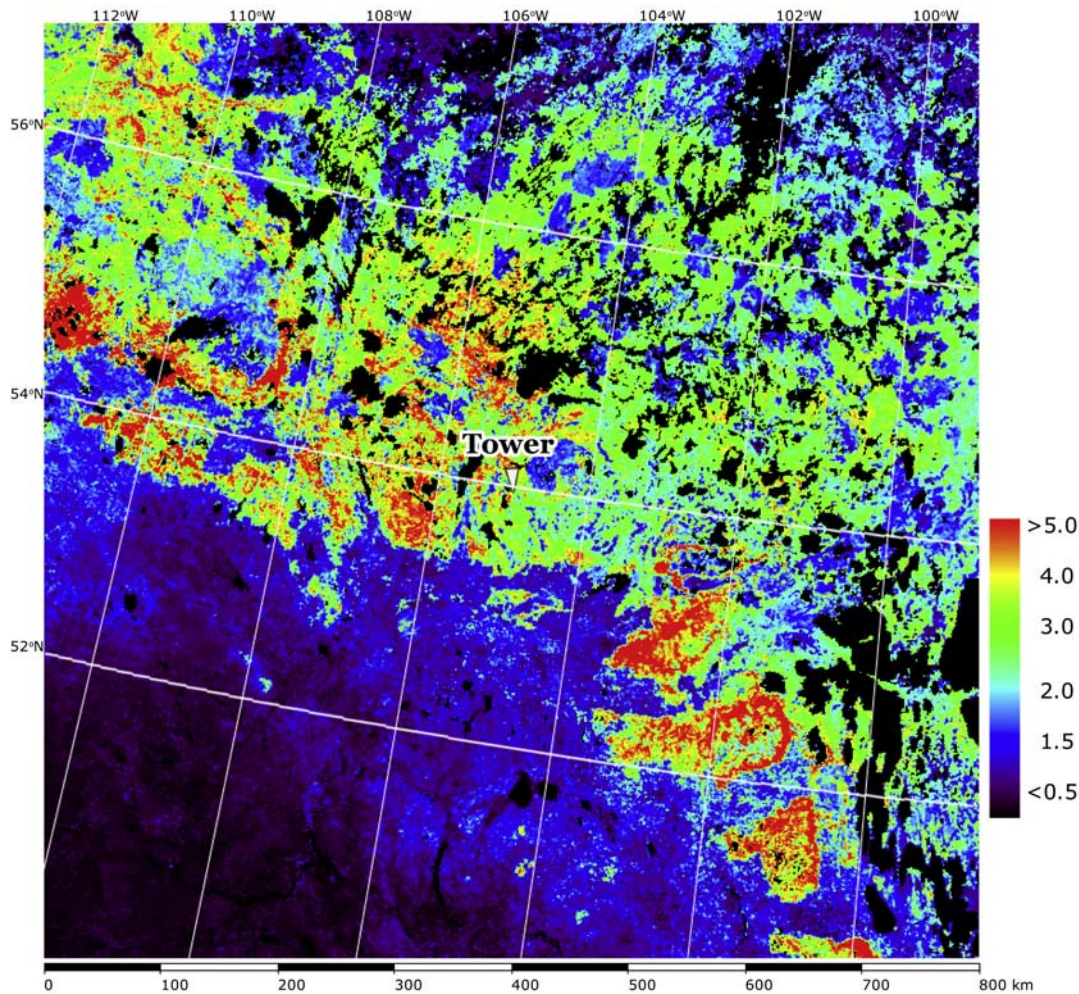


**Figure 2.** Leaf area index (LAI) map for the region surrounding the SOBS tower for the first 10 d of August 2003.

mesoscale circulations (e.g., sea/lake breezes) and boundary layer cloud formulation tend to counter the influence of the land surface by facilitating mixing between the PBL and the typically drier and warmer overlying troposphere [Helliker *et al.*, 2004]. The PBL air mass moves over the terrestrial surface ( $\sim 500 \text{ km d}^{-1}$  under typical fair weather conditions), dispersing trace gases horizontally and vertically due to divergence and wind shear [Raupach *et al.*, 1992]. Hence, the air composition in the surface layer is determined by the initial composition of the air mass and the exchanges with the underlying surface and the overlying free troposphere [Helliker *et al.*, 2004]. It has been noted from three-dimensional atmospheric transport model simulations [e.g., Fung *et al.*, 1983] that meridional transport can result in substantial displacement of the actual change in the atmospheric burden of  $\text{CO}_2$  in latitudinal zones from the corresponding surface fluxes that drove them. The influence of large-scale atmospheric transport on  $\text{CO}_2$  concentration in the atmospheric boundary layer is hence expected, and this should interact with concentration gradients generated by regional exchange with the surface. Suppose we want to estimate surface fluxes in a given region (e.g., the daily

concentration footprint area), on the basis of mass conservation, the atmospheric concentration of a gas (e.g.,  $\text{CO}_2$ , expressed as  $C$ ) measured in a terrestrial tower at a reference height (observed values, i.e., in the land surface layer) reflects the combination of some background atmospheric concentration and variable amounts of that gas added from sources in both the vertical and horizontal directions:

$$C_{\text{obs}} = C_{\text{bg}} + \Delta C_{\text{surf}} + \Delta C_{\text{adv}}, \quad (1)$$

where  $C_{\text{obs}}$  and  $C_{\text{bg}}$  are, respectively, the observed atmospheric  $\text{CO}_2$  concentration at a reference site and the background value;  $\Delta C_{\text{surf}}$  is the change in the  $\text{CO}_2$  mixing ratio caused by local surface fluxes of carbon, which might result mostly from local biological activities, biomass burning and the fossil fuel combustion;  $\Delta C_{\text{adv}}$  is the change in the  $\text{CO}_2$  mixing ratio due to advection resulting from a horizontal  $\text{CO}_2$  gradient. Equation (1) works in many time frames, e.g., hourly, daily, and monthly. The  $\text{CO}_2$  mixing ratios in terrestrial ecosystems are also found to be dominated by biological activities during the growing season under the condition that the upwind ecosystems

behave in a very uniform way [Bakwin *et al.*, 1998; Potosnak *et al.*, 1999]. In this study, we tried to explore a simple method to infer regional GPP in daily time steps from continuous CO<sub>2</sub> mixing ratio measurements in the surface layer using a 1-D model. We therefore assume that  $\Delta C_{\text{adv}}$  can be ignored since  $\Delta C_{\text{surf}} \gg \Delta C_{\text{adv}}$  in the daily short time frame.

[12] The boundary layer interacts with the surface (including horizontal advection) and the background atmosphere on similar time frames. While changes in the atmospheric background CO<sub>2</sub> by many factors, such as advection, deep convection, subsidence, etc., are normally much slower than that in measured surface CO<sub>2</sub>. The relaxation time of changes in the background atmospheric CO<sub>2</sub> (i.e., the CO<sub>2</sub> concentration in free troposphere in this study) is much longer than that in the PBL driven by the exchange of CO<sub>2</sub> with the surface in the daily concentration footprint area (about 1 order longer, e.g., 10 d versus 1 d). Hence, the background CO<sub>2</sub> changes could be ignored.

[13] We also neglected the difference between the free tropospheric CO<sub>2</sub> value and value observed within the marine boundary layer (“MBL reference”). The MBL reference CO<sub>2</sub> [Masarie and Tans, 1995] is a weekly varying concentration field with spatial increment of 0.05 sine of latitude constructed from observations within the MBL [Globalview-CO<sub>2</sub>, 2005]. We used the MBL reference for free troposphere because of the absence of direct observations, though observations from the high observational density from intensive field sampling programs showed significant deviations of free tropospheric concentrations from the MBL references in some regions over the continent. However, during the daytime, the change in free tropospheric CO<sub>2</sub> is expected to be small. It is the daytime change that affects the deviation of daily GPP.

### 3.2. Method 1: PBL Carbon Budget Analysis

#### 3.2.1. An Integrated Ecosystem-Boundary Layer Model for Estimating Ecosystem Fluxes and Atmospheric Diffusion

[14] In order to isolate photosynthesis signals from atmospheric CO<sub>2</sub> data, we employed an integrated ecosystem-boundary layer model to simulate dynamics of CO<sub>2</sub> in the PBL. This model consists of two components: (1) an ecosystem model (BEPS: the Boreal Ecosystem Productivity Simulator) [Chen *et al.*, 1999; Liu *et al.*, 1999, 2002]; and (2) a one-dimensional atmospheric model (VDS: Vertical Diffusion Scheme) [Chen *et al.*, 2004; B. Chen *et al.*, 2005].

[15] The version of BEPS used in this study is a new version that includes a land surface scheme: Ecosystem-Atmosphere Simulation Scheme (EASS) [B. Chen *et al.*, 2007]. It has the following characteristics: (1) satellite data are used to describe the spatial and temporal information on vegetation, and in particular, we use a foliage clumping index ( $\Omega$ ) in addition to LAI to characterize the effects of three-dimensional canopy structure on radiation, heat and carbon fluxes; (2) energy and water exchange and carbon assimilation in soil-vegetation-atmosphere systems are fully coupled and are simulated simultaneously; and (3) the energy and carbon assimilation fluxes were calculated with stratification of sunlit and shaded leaves to avoid short-

comings of the “big-leaf” assumption. This updated version has been systematically validated using eddy covariance flux data [Ju *et al.*, 2006; B. Chen *et al.*, 2007] at Canadian forest sites and used for upscaling land surface fluxes [J. M. Chen *et al.*, 2007] and isotope studies [B. Chen *et al.*, 2006a, 2006b; Chen and Chen, 2007].

[16] VDS is a one-dimensional bottom-up and top-down vertical mixing model [Chen *et al.*, 2004; B. Chen *et al.*, 2005] similar to those of Wyngaard and Brost [1984] and Moeng and Wyngaard [1989] simulating the transport processes of scalar entities (e.g., CO<sub>2</sub>, temperature) from the surface layer up to the top of PBL. VDS has two different schemes (modules) to treat different situations of the PBL structures (stable boundary layer: SBL or convective boundary layer: CBL) [Chen *et al.*, 2004; B. Chen *et al.*, 2005]. The selection of a stable or free convection scheme is determined by atmospheric stability. In VDS, the mixed layer is stratified into 50-m thick layers and constant bottom-up and top-down mixing coefficients are used throughout the PBL at a given time [Zhang and Anthes, 1982]. This model configuration allows CO<sub>2</sub> concentration in each layer to vary with time according to the vertical concentration gradient and the mixing coefficients at each time step (30 s) in stead of using the quasi-steady state assumption for the vertical gradient [Moeng and Wyngaard, 1989]. The integrated ecosystem-boundary layer model is forced by the near-surface meteorological variables, including air temperature, air relative humidity, incoming short-wave radiation, wind speed, and precipitation. The land surface data, including vegetation (i.e., LC, LAI) and soil data are also needed as model inputs. Most vegetation parameters were derived from satellite images. As shown in Figures 1 and 2, LC and LAI were derived from satellite images at a 1-km resolution (directly from VEGETATION images, or up-scaling from Landsat TM) [Chen *et al.*, 2002]. The LAI map is generated with 10-d intervals with annual total of 36 maps.  $\Omega$  was derived from multiangular POLDER 1 data [J. M. Chen *et al.*, 2005]. Data on soil texture (sand, silt and clay fractions) and carbon pools are obtained from the Soil Landscapes of Canada (SLC) database, version 1.0 and 2.0 [Shields *et al.*, 1991; Schut *et al.*, 1994; Lacelle, 1997]. For the one-dimensional BEPS-VDS simulations, the average values of LAI and  $\Omega$  near the SOBS (a radius of 1 km) are obtained from these maps, and the LC type is taken as the dominant type of conifer. For estimating the entrainment of CO<sub>2</sub> at the top of the mixed layer, the background atmospheric value (i.e., the free tropospheric CO<sub>2</sub>) is needed for the top condition of our one-dimensional model. As mentioned above, we use the latitudinally interpolated MBL CO<sub>2</sub> as a substitute for the free troposphere.

#### 3.2.2. Method for Deriving Daily GPP From CO<sub>2</sub> Concentration Measurements

[17] As the air CO<sub>2</sub> mixing ratio at a given height is determined by both the surface metabolism and atmospheric mixing processes. It would be possible to isolate the signals for the metabolism if atmospheric diffusion is accurately modeled. This requires that both the exchange of CO<sub>2</sub> between the ecosystem and the atmosphere and the atmospheric transport within the PBL are accurately simulated.

This integrated ecosystem-boundary layer model (BEPS-VDS) simulated well the surface fluxes (both photosynthesis and respiration) and the concentration of CO<sub>2</sub> in the surface layer (see section 4). After the first “normal” model run, we implement a hypothetical model run by switching off GPP in the model, i.e., setting GPP = 0. In the this run, only the GPP produced by BEPS is set to zero while keeping all other hourly fluxes unchanged from the previous run, including respiration and entrainment. A new CO<sub>2</sub> profile produced in the second model run is purely driven by  $R$ , which is simulated by BEPS for the grid cell around the tower. The reduction of observed CO<sub>2</sub> from the simulated values at the measurement height is entirely due to GPP, that is, the amount of the reduction is the part of CO<sub>2</sub> removed by GPP. The signals of GPP are hence isolated by “turning off” the GPP in BEPS and quantifying the accumulated air CO<sub>2</sub> decrease (the difference between the observed and simulated values with GPP = 0) from dawn to dusk. Near dusk, the planetary boundary layer is still well mixed, so this increase in CO<sub>2</sub> can be converted into GPP using boundary layer CO<sub>2</sub> mass budgeting. This methodology has been applied to a 13-year CO<sub>2</sub> record observed on the Fraserdale tower, Ontario, Canada, to study the temperature effect on the boreal carbon cycle [J. M. Chen *et al.*, 2006; B. Chen *et al.*, 2006a, 2006b] and validated using simultaneous CO<sub>2</sub> flux and concentration data at the WLEF tall tower (Wisconsin, United States [J. M. Chen *et al.*, 2007]).

### 3.3. Method 2: Remote Sensing Based Footprint Integration

#### 3.3.1. An Analytical Scalar Concentration Footprint Model

[18] The scalar concentration footprint “source” area is the “view of the concentration sensor” on a tower. The scalar concentration footprint function ( $f$ ) describes the flux portion “seen” by the scalar concentration sensor. Our concentration footprint model is a modified version of that of Schmid [1994]. All upwind sources encompassed by the measurement point at a height ( $z_m$ ) above the ground potentially contribute to the measured scalar concentration ( $C$ ). The measured departures of CO<sub>2</sub> concentration from the background values  $C_{bg}$ , therefore, is the result of an integration of the product of the surface flux ( $F$ , in  $\mu\text{mol m}^{-2} \text{s}^{-1}$ ) and footprint function ( $f$ ) over the entire upwind source area:

$$C(0, 0, z_m) = C_{bg} + \int_{-\infty}^{\infty} \int_{-\infty}^{\infty} F(x, y, 0) f(x, y, z_m) dx dy, \quad (2)$$

where  $C$  is in  $\mu\text{mol m}^{-3}$ ;  $f$  is in  $\text{s m}^{-3}$ ;  $x$  is the stream-wise distance in meters; and  $y$  is the crosswind distance from the center line in meters.

[19] The scalar concentration footprint function (i.e., the downwind concentration distribution of a unit point source (plume) occurring at the origin ( $x = y = 0, z \geq 0$ )) is the product of the crosswind-integrated concentration footprint,

$f^y$  in  $\text{s m}^{-2}$ , and the crosswind distribution function  $D_y$  in  $\text{m}^{-1}$  [Pasquill, 1974; van Ulden, 1978; Horst and Weil, 1992],

$$f(x, y, z_m) = D_y(x, y) f^y(x, z_m). \quad (3)$$

Dispersion in the lateral ( $y$ ) direction is calculated as a Gaussian function [Pasquill, 1974],

$$D_y(x, y) = \frac{1}{\sqrt{2\pi}\sigma_y} \exp\left(-\frac{y^2}{2\sigma_y^2}\right), \quad (4)$$

where  $\sigma_y$  is the standard deviation of the plume in the  $y$  dimension, depending on atmospheric stability and upwind distance ( $x$ ). In accordance with the short-range limit of statistical turbulence theory [Pasquill, 1974; Schmid, 1994],  $\sigma_y$  is approximated as  $\sigma_y x / \bar{u}$ , where  $\sigma_v$  is the standard deviation of lateral wind fluctuations.

[20] The crosswind-integrated concentration footprint,  $f^y$  at the upwind distance  $x$  is described as

$$f^y(x, z_m) = \frac{D_z(x, z_m)}{\bar{u}(x)}, \quad (5)$$

where  $D_z$  is the vertical concentration distribution function in  $\text{m}^{-1}$  and  $\bar{u}$  is the effective velocity of the plume in  $\text{m s}^{-1}$ ;  $\bar{u}$  is forced by mass conservation to be

$$\bar{u}(x) = \int_0^{\infty} u(z) D_z(x, z) dz, \quad (6)$$

where  $u(z)$  is the horizontal wind velocity in  $\text{m s}^{-1}$ . Following an analytical solution of Eulerian advection-diffusion equation by van Ulden [1978],  $D_z$  is expressed as

$$D_z(x, z_m) = \frac{A}{\bar{z}(x)} \exp\left[-\left(\frac{Bz}{\bar{z}(x)}\right)^r\right], \quad (7)$$

where  $\bar{z}$  is the mean plume height; the coefficients  $A$  and  $B$  equal  $r\Gamma(2/r)/\Gamma(1/r)^2$  and  $\Gamma(2/r)/\Gamma(1/r)$ , respectively;  $\Gamma$  is the Gamma function and  $r$  is a shape parameter and  $r = 2 + m - n$ , where  $m$  and  $n$  are the exponent of the wind velocity power law and the exponent of the eddy diffusivity power law, respectively;  $u(z) = Uz^m$  and  $K(x) = kz^n$ , where  $U$  and  $k$  are the effective speed of plume advection and an effective eddy diffusivity coefficient, respectively. For mathematical simplicity, we need to explicitly express  $\bar{z}(x)$  and  $\bar{u}(x)$  to solve equations (5) and (7) by integration of equation (13) of van Ulden [1978] as

$$\bar{z}(x) = B \left(\frac{r^2 k}{U}\right)^{1/r} x^{1/r}, \quad (8a)$$

$$\bar{u}(x) = \frac{\Gamma((1+m)/r)}{\Gamma(1/r)} \left(\frac{r^2 k}{U}\right)^{m/r} U x^{m/r}. \quad (8b)$$

[21] This is a very Simple Analytical Footprint model on Eulerian coordinates (SAFE). On the basis of the K-theory and assuming horizontally homogeneous turbulence, an analytical solution of  $f(x, y, z_m)$  is obtained from the functional form of the concentration distribution and the shape of the wind profile (equation (3)). The dimensions and orientation of  $f(x, y, z_m)$  depend on the location and height of the sensor, wind direction, wind velocity, surface roughness, and atmospheric stability.

[22] Footprint estimates can be classified as stochastic Lagrangian, analytical approaches, or large-eddy simulations. Lagrangian models can be applied in any turbulence regime (even in inhomogeneous or nonstationary conditions), while most analytical models are constrained to homogeneous turbulence. The values of the upwind tail of concentration footprint estimated by a three-dimensional Lagrangian stochastic dispersion model are generally higher than those by an analytical footprint model [Kljun *et al.*, 2003]. At these large separation distances between the source and the receptor, the mean plume height could be well above the surface layer, and thus beyond the validity range of the K-theory-based analytical model. To avoid the model biases resulting from the limitation of our analytical model, we neglected the very small contribution from the long upwind tail. In the model implementation, we simply sort  $f(x, y, z_m)$  values in a descending order and then accumulate the values from the largest to the smallest until a given fraction  $\Pi$  is achieved. The source area  $\Omega_{\Pi}$  includes all grids (pixels) that have  $f(x, y, z_m)$  larger than the cutoff point, and the fraction  $\Pi$  is the ratio of the cumulative footprint function within  $\Omega_{\Pi}$  to the whole integrated source function,

$$\Pi = \frac{\varphi_P}{\varphi_{\text{tot}}} = \frac{\iint_{\Omega_P} f(x, y, z) dx dy}{\iint_{-\infty}^{\infty} \iint_{-\infty}^{\infty} f(x, y, z) dx dy}, \quad (9)$$

where  $\varphi_P$  and  $\varphi_{\text{tot}}$  are the integrals of the footprint function over  $\Omega_{\Pi}$  and the total area, respectively. In this study, we set  $\Pi$  to 0.90. The footprint function  $f(x, y, z_m)$  at every grid point within  $\Omega_{\Pi}$  is then normalized by the integral of the footprint function over  $\Omega_{\Pi}$  for each day to yield the daily weighted footprint function ( $\phi$ ),

$$\phi(x, y) = f(x, y, z_m) dx dy / \iint_{\Omega_P} f(x, y, z_m) dx dy. \quad (10)$$

The integral of daily weighted footprint function ( $\phi$ ) equals 1.

[23] The SAFE model was coupled with EASS. The sensible heat flux simulated by EASS is needed for calculating the atmospheric stability in SAFE. SAFE needs the same model inputs as BEPS (see section 3.2.1) with the additional input of hourly wind direction and its deviation.

**3.3.2. Method of Calculating Regional Net CO<sub>2</sub> Flux on the Basis of Footprint Estimation and Ecosystem Modeling**

[24] The surface flux information contained in CO<sub>2</sub> concentration measured at the tower ( $F_{\text{region}}$ ) is the integration of

surface CO<sub>2</sub> flux ( $F$ ) weighted with concentration footprint function ( $\phi$ ) for each pixel over the upwind footprint source area ( $\Omega_{\Pi}$ ),

$$F_{\text{region}} = \iint_{\Omega_P} F(x, y) \phi(x, y) dx dy. \quad (11)$$

The surface CO<sub>2</sub> flux  $F(x, y)$  can be net CO<sub>2</sub> flux or any component of carbon fluxes, i.e., GPP or  $R$ . In this study, we focus on GPP. The spatially explicit BEPS model was used to simulate GPP at 1 km resolution over the concentration footprint area of the SOBS tower. The daily concentration footprint function ( $\phi$ ) for each pixel (same size as BEPS) was simulated using SAFE.

### 3.4. Method for Deriving Local GPP From EC Measurements

[25] The surface flux was calculated as the sum of the eddy flux, measured at 25 m, and the rate of change of storage in the air column below the flux measurement level. The surface CO<sub>2</sub> flux provides a direct measurement of the net ecosystem exchange ( $F_{\text{NEE}}$ )—the net exchange rate of CO<sub>2</sub> between the ecosystem and the atmosphere. Following Barr *et al.* [2004], two adjustments were applied to  $F_{\text{NEE}}$ : the nighttime  $F_{\text{NEE}}$  data were excluded at low  $u_*$  (here,  $u_* < 0.35 \text{ m s}^{-1}$ ) and an energy-balance-closure adjustment was applied by dividing the measured  $F_{\text{NEE}}$  by the fractional energy balance closure (here, 89%), calculated as the ratio of the sum of the sensible and latent heat fluxes to the available energy flux.  $F_{\text{NEE}}$  provides a direct measure of the net ecosystem production ( $F_{\text{NEP}} = -F_{\text{NEE}}$ ). At local scale (i.e., EC flux footprint area),  $F_{\text{NEP}}$  results as the difference between carbon gains by GPP and carbon losses by  $R$  (i.e.,  $F_{\text{NEP}} = \text{GPP} - R$ ). Positive values of  $F_{\text{NEP}}$  correspond to CO<sub>2</sub> uptake by the ecosystem.

[26]  $R$  and GPP were partitioned from  $F_{\text{NEP}}$  measurements. The measured  $R$  was estimated as  $R = -F_{\text{NEP}}$  during periods when GPP was known to be zero, i.e., growing-season nighttime and non-growing-season (periods when both air ( $T_a$ ) and 2-cm soil ( $T_s$ ) temperatures were lower than 0°C). GPP was obtained from measured  $F_{\text{NEP}}$  and estimated daytime  $R_d$  as  $\text{GPP} = F_{\text{NEP}} + R_d$ . The core of this methodology was to first derive simple annual empirical relationships (for example,  $R_d = f(T_s)$ ) from measured data.  $R_d$  values were estimated from an empirical logistic equation (fitted to the measured  $R$  values from the entire year [Barr *et al.*, 2004],

$$R_d = f(T_s, t) = \frac{r_1(t)r_1}{1 + \exp(r_2(r_3 - T_s))}, \quad (12)$$

where  $T_s$  is soil temperature at the 5-cm depth;  $r_1$ ,  $r_2$ , and  $r_3$  are the empirical parameters, held constant over the year; and  $r_1(t)$  is a time-varying parameter. The values of  $r_1(t)$  were estimated within a 100-point moving window as the

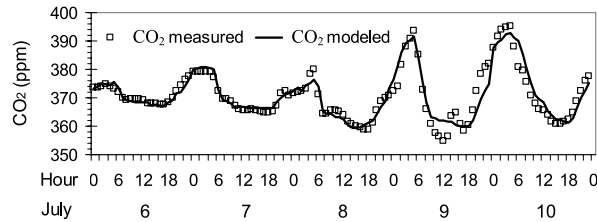


**Figure 3.** Comparison of measured (symbols) and modeled (solid line) CO<sub>2</sub> mixing ratios for 6–10 July 2003.

slope of a linear regression (forced through zero) of the modeled  $R$  estimates from (equation (12)) versus measured  $R$ .

## 4. Results

### 4.1. Atmospheric Diffusion and Ecosystem Modeling

[27] A critical step in our methodology of extracting the photosynthesis signal from the CO<sub>2</sub> record is to ensure that atmospheric diffusion is simulated with a reasonable accuracy. Although the integrated ecosystem-boundary layer model has been shown to perform well in the previous studies [Chen *et al.*, 2004; B. Chen *et al.*, 2005, 2006a, 2006b; J. M. Chen *et al.*, 2007], model validation of simulated CO<sub>2</sub> mixing ratio against measurements at this SOBS tower was also made in this study. Figure 3 provides examples of the simulated CO<sub>2</sub> mixing ratios in comparison with observed values for five consecutive days in July 2003. The simulated curves generally followed the observed values closely, even though the simulation was made with a simple one-dimensional model. The simulated curves were generally smoother than the observed values because of the assumption of horizontal homogeneity used in the 1-D model. There were synoptic events (frontal systems) causing abrupt changes in CO<sub>2</sub> concentration, and simulated values from the 1-D model had the largest departure from measurements under these circumstances (e.g., 9 July, as shown in Figure 3). Similar simulation results were obtained for all days in 2003, and the results were summarized in Table 1 in terms of regression statistics between modeled and observed CO<sub>2</sub> concentrations. The  $r^2$  value increases and the root mean square error (RMSE) decreases as the modeled hourly values are averaged for daily and 10-d

**Table 1.** Statistics for the Regression Between Modeled and Observed CO<sub>2</sub> Concentrations on the SOBS Tower for Hourly, Daily, and 10-d Mean Values<sup>a</sup>

	$r^2$	RMSE (ppm)	Sample Size (n)
Hourly	0.67	4.8	6910
Daily	0.73	2.3	291
10 d	0.87	2.1	36

<sup>a</sup>The  $r^2$  is the linear regression coefficient, and RMSE is the root mean

square error,  $= \sqrt{\frac{1}{n} \sum_{i=1}^n [C_{\text{mod}}(i) - C_{\text{obs}}(i)]^2}$ .

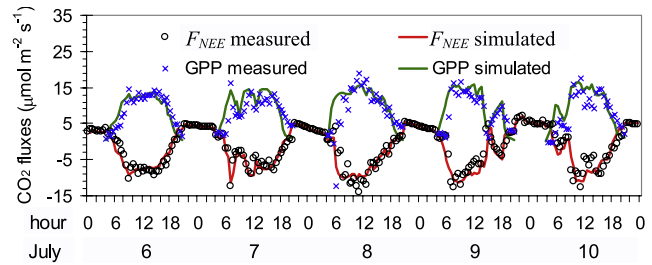


**Figure 4.** Comparison of the EC-measured half-hourly net ecosystem exchange ( $F_{\text{NEE}}$ ) and EC flux derived GPP with BEPS simulated half-hourly net ecosystem exchange ( $F_{\text{NEE}}$ ) and GPP for 6–10 July 2003.

periods, suggesting that the 1-D model can generally capture the underlying ecosystem variability for regional carbon balance estimation.

[28] To ensure that atmospheric diffusion is simulated with an acceptable accuracy for our purpose of using a CO<sub>2</sub> record for deriving ecosystem information, we should also have the first order estimate of the CO<sub>2</sub> flux to and from the underlying the surface. Figure 4 shows comparison of the EC-measured  $F_{\text{NEE}}$  and GPP derived from EC flux measurements with simulated  $F_{\text{NEE}}$  and GPP for the same period as shown in Figure 3. The model simulations generally had good agreement with observations.

[29] After gaining confidence in modeling the atmospheric diffusion and ecosystem metabolism, we applied the methodology illustrated in section 3.2.2 and J. M. Chen *et al.* [2007] to the entire record of CO<sub>2</sub> in 2003. Daily GPP values were computed from the hourly CO<sub>2</sub> concentration for the whole year (see section 4.4).

### 4.2. Estimates of Daily Concentration Footprint

[30] SAFE was applied to the SOBS tower for 2003. To be compatible with BEPS, the grid size in SAFE was set to be 1 km × 1 km. The calculated footprints are shown in Figure 5 for four arbitrary days in 2003. The parameters for characterizing the daily mean wind and atmospheric stability for these 4 d are listed in Table 2. The footprint peak was about 10 km upwind of the tower, and the upwind tail within the cutoff point extended up to 250–350 km depending on weather conditions (Figure 5a). The crosswind distribution followed the assumed Gaussian distribution, but the decline rates from the peak isopleth depended on the atmospheric stability and the standard deviation of the lateral spread (Figure 5b). Different days had different footprints (Figures 6a and 6b) as the air flowed from different directions with different widths of dispersion. The northwest winds contributed the most to the annual footprint for the SOBS tower in 2003, while northeast winds contributed the least (Figure 7).

### 4.3. Simulated GPP Field at 1 km Resolution

[31] The spatially explicit BEPS model was used for simulating the GPP over the concentration footprint area of the SOBS tower. Values of the daily total GPP at 1 km resolution for 11 and 24 August were shown in Figures 6c



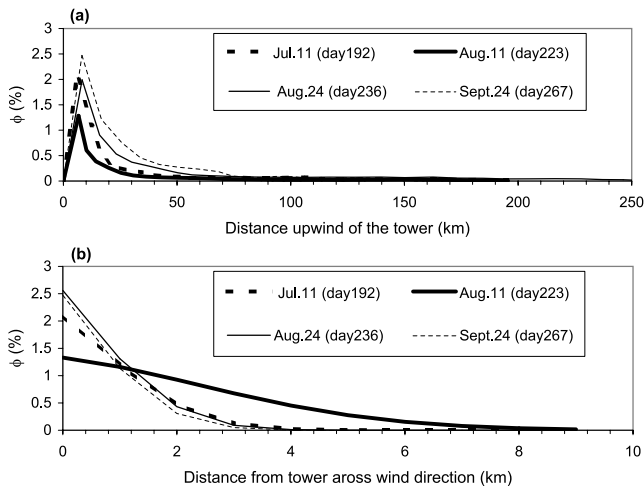


**Figure 5.** Simulated concentration footprint cross sections for four arbitrary days in 2003. (a) Along the wind direction and (b) across the wind direction from center line of the mean flow. The parameters for characterizing the daily mean wind and atmospheric stability are listed in Table 2.

and 6d, as examples. The differences between these 2 d were apparent. On the basis of the simulated daily GPP and daily weighted concentration footprint, we calculated the daily regional GPP values that influence the concentration measurements at the tower using equation (11) for the whole year (Figure 9).

#### 4.4. Comparison of GPP Estimates

[32] In order to test the performance of BEPS, model parameters were not “tuned” to obtain a better match with the tower observations, and the land surface inputs were derived from remote sensing images instead of using the measurements. As shown in Figure 8, the simulated daily GPP in the 1 km pixel containing the SOBS tower generally followed the EC flux derived GPP ( $r^2 = 0.76$ ) well because they represent the similar local source area (EC flux footprint area: about 1 km<sup>2</sup> surrounding the tower), but the model tends to underestimate the measured GPP in the middle growing season. Estimates of GPP using the PBL-budget method are likely representative of a regional scale owing to the large source area that affects the mixing ratio (concentration footprint area: about 10<sup>3</sup>–10<sup>5</sup> km<sup>2</sup>). The source areas are the same in the PBL-budgeting (method 1) and the concentration-footprint-integrating (method 2) approaches. The estimates of daily GPP by these two approaches were compared in Figure 9. The PBL-budgeted estimates were in good agreement with the concentration-footprint-integrated estimates (slope = 0.99;  $r^2 = 0.89$ ). In order to test these methods to infer the regional GPP from mixing ratio measurements, we also compared the estimates of regional GPP with EC flux derived GPP although their source areas are different. Regression analysis revealed that they were highly correlated but concentration-derived daily GPP only reached about 80% of the magnitudes of EC flux derived daily GPP (Figure 10). The seasonal patterns of the weekly averages of GPP

estimated by these four approaches (at both local and regional scales) were quite similar although the spatial scales represented by these four sets of estimates were very different (Figure 11). Similar to regression analysis at daily time steps (Figure 10), we also see from Figure 11 that the regional GPP estimates were consistently much smaller than the local GPP for all days in 2003. This is consistent with characteristics of the source areas (different land cover types) represented by these two quantities. The EC flux footprint area (local GPP) is dominated by a black spruce forest while the concentration footprint areas (regional GPP) include forest, shrub, grass, agriculture crop fields and open water bodies, all of which are likely to be less productive. Seasonal budgets of GPP estimates were summarized in Table 3 and Figure 12. The estimates of annual GPP were about 819–847 g C m<sup>-2</sup> for the smaller area surrounding the tower and 649–664 g C m<sup>-2</sup> for the region around the tower, respectively. The differences in GPP estimates by different methods for the similar spatial scales were within 4%. The regional estimates were about 20–25% lower than the local estimates and most of the differences occurred during the early to middle growing season (i.e., May to July, Figure 12).

## 5. Discussion

[33] This study makes use of measurements of the high-frequency CO<sub>2</sub> mixing ratio on a short tower to estimate the net CO<sub>2</sub> exchange at daily or longer timescales. The PBL dynamics naturally integrate the effects of land ecosystems on the atmosphere at a regional scale. Because of the convective boundary layer (CBL) dynamics, the influence of the inhomogeneous surface on the atmospheric CO<sub>2</sub> is smoothed, and the evolution of atmospheric CO<sub>2</sub> with time in a day represents the integrated influence of the surface flux over the concentration footprint. The surface area that influences the PBL for 1 d is estimated to be about 10<sup>4</sup> km<sup>2</sup> [Raupach *et al.*, 1992]. Mixing within the CBL occurs rapidly (~15 min) relative to the timescale for substantial changes in surface fluxes (~1 h except near sunrise and sunset). This allows simple mass-balance approaches to relate average CBL concentrations to the surface flux [Styles *et al.*, 2002]. The daily GPP extracted from hourly CO<sub>2</sub> concentration measurements (method 1) should represent the upwind area of the tower in the mean wind direction on a given day. The daily concentration footprint area was estimated to be around 10<sup>3</sup>–10<sup>4</sup> km<sup>2</sup>, smaller than 10<sup>4</sup>–10<sup>5</sup> km<sup>2</sup> for

**Table 2.** Parameters for Characterizing the Wind and Atmospheric Stability for the Four Arbitrary Days as Shown in Figure 5<sup>a</sup>

	$u$ (m s <sup>-1</sup> )	$\sigma_v$ (m s <sup>-1</sup> )	$\sigma_d$ (degrees)	$u^*$ (m s <sup>-1</sup> )	$1/L$ ( $\times 10^{-3}$ ) (m <sup>-1</sup> )	$R_b$
11 Jul	3.3	1.8	20.4	0.48	-9.9	0.15
11 Aug	3.7	2.6	25.1	0.53	-30.8	0.08
24 Aug	5.2	2.2	14.8	0.74	-1.6	0.05
24 Sep	3.9	2.3	15.7	0.54	-3.2	0.05

<sup>a</sup>Where  $u$  is the wind velocity,  $\sigma_v$  is the standard deviation of lateral wind velocity fluctuations,  $\sigma_d$  is the standard deviation of lateral wind directions,  $u^*$  is the friction wind speed,  $1/L$  is the reciprocal of Obukhov length, and  $R_b$  is the bulk Richardson number.

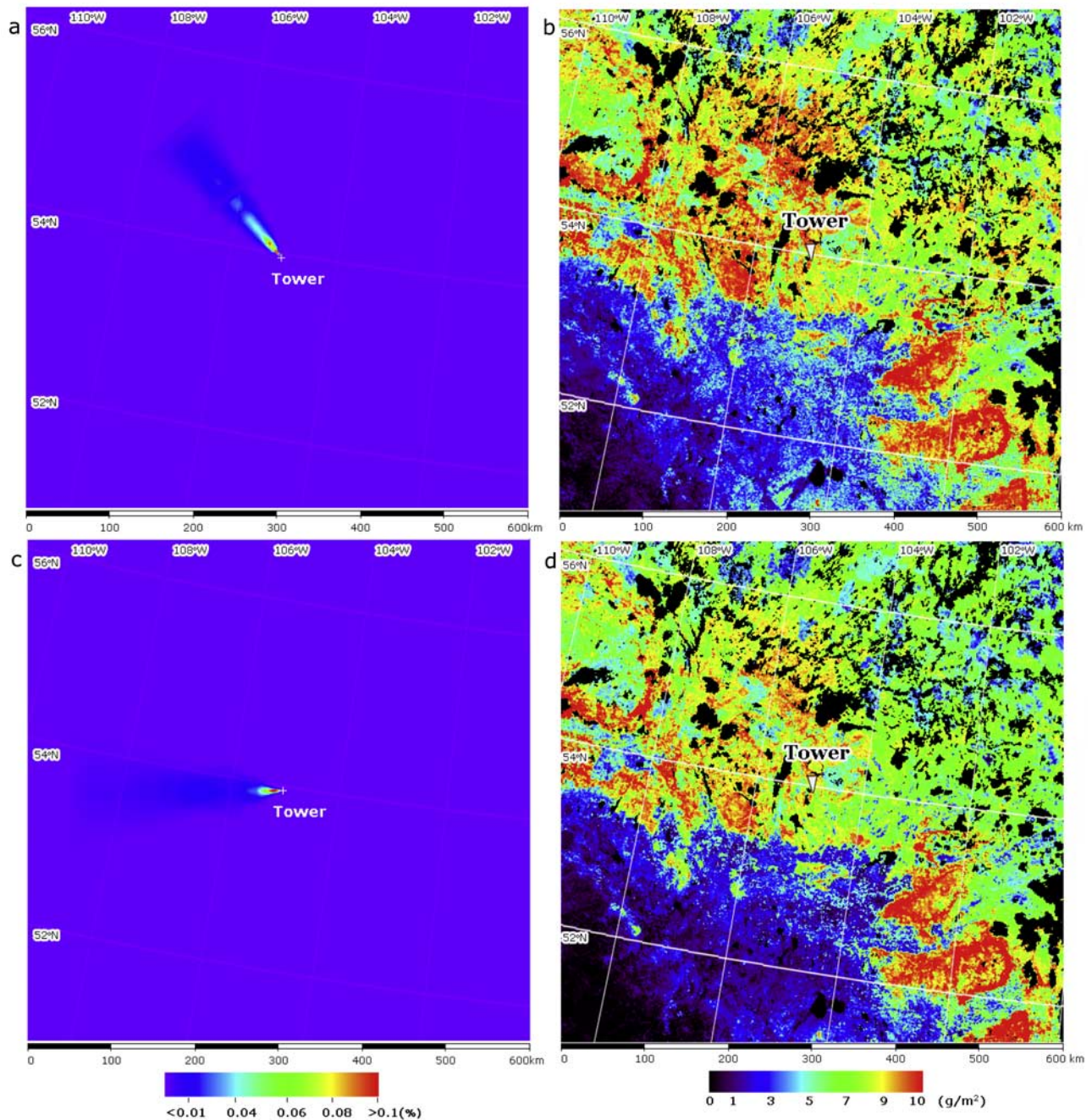


**Figure 6.** Simulated footprint and gross primary productivity (GPP) maps at 1 km resolution on two arbitrary days. (a) The footprint and (b) GPP maps for 11 August 2003. (c, d) The corresponding maps for 24 August 2003.

multiple days [Gloor *et al.*, 2001; Lin *et al.*, 2004]. Though it is difficult to separate the near-field and the far-field effects on the estimated daily GPP using our methodology, the far-field effect on daily GPP estimation is quite small. We therefore expect the biases in estimated daily GPP by neglecting the change in background atmospheric  $\text{CO}_2$  in our one-dimensional ecosystem-boundary layer model are not significant.

[34] Moreover, satellite data provide independent information on the spatial and phenological variations of GPP

using an ecosystem model such as BEPS. Given a reasonable estimate of the actual footprint under certain micro-meteorological conditions and a simulation of the surface flux field by BEPS based on remote sensing, we can calculate the daily regional GPP values that influence the concentration measurements using equation (11) (method 2). This is an effective method to retrieve the regional carbon flux information which is “seen” by the concentration sensor on the tower.

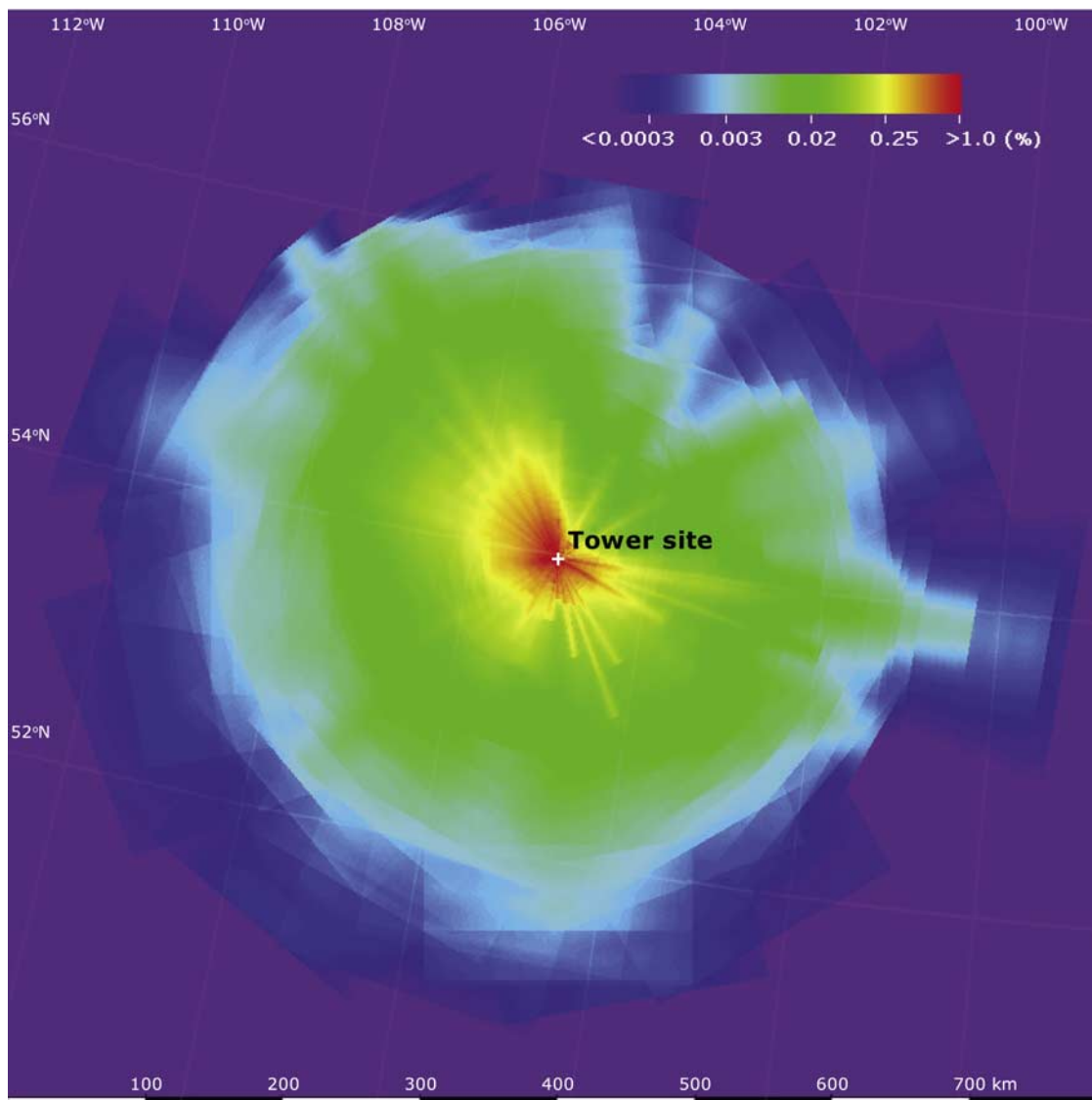


**Figure 7.** Annual concentration footprint for the SOBS tower for 2003.

[35] The PBL carbon budget (i.e., concentration-derived) method uses a one-dimensional ecosystem-boundary layer model. By “turning off” the modeled GPP and estimating the actual GPP through PBL budgeting from the accumulated increase in  $\text{CO}_2$  concentration, modeled after GPP is “turned off”, from the observed  $\text{CO}_2$  concentration at sunset, we greatly reduce the error due to surface heterogeneity. However, this methodology does not tell which the source area the concentration-derived GPP represents. As the air flows from different directions over different underlying surfaces, large day-to-day variations are expected even though the micrometeorological conditions are similar. The combination of concentration footprint estimation with remote sensing based GPP estimation provides an opportunity to evaluate the reliability of the concentration-derived GPP as it explicitly considers the source areas for the concentration measurements. The significance of concentration-derived flux information is its large concentration

footprint consisting of many cover types of different vegetation densities, and so far there has been no other ways to validate carbon cycle information derived from atmospheric  $\text{CO}_2$  mixing ratio measurements.

[36] In this study, these two independent regional GPP estimates showed close agreement. However, it must be realized that it is still possible that both of them have similar biases, i.e., simultaneously overestimated or underestimated. We assume the MBL reference  $\text{CO}_2$  as a substitute for background value (free tropospheric value) for the two methods. The departures of free tropospheric concentrations from MBL reference over the continent was reported to be  $\sim 3$  ppm in some regions, with an averaging value of  $\sim 1$ – $2$  ppm according to the  $\text{CO}_2$  Budget and Rectification Airborne study (COBRA) measurements [Gerbig *et al.*, 2003; Lin *et al.*, 2004, 2006]. Such systematic departures can be explained in large part by advection from different latitudes and by time lags in vertical propagation of con-

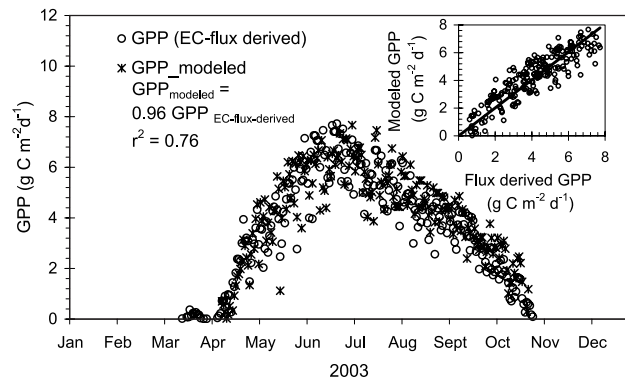


**Figure 8.** Comparison of BEPS simulated daily GPP of the  $1 \times 1$  km pixel which contains the SOBS tower with that derived from EC flux measurements. The inset shows the linear regression between these two GPP estimates.

centration changes at the surface, within the MBL, to the free troposphere [Gerbig *et al.*, 2003]. A typical vertical  $\text{CO}_2$  gradient (PBL-free troposphere) was larger than 10 ppm during summer growing season in the research area. Suppose the difference in  $\text{CO}_2$  concentration between free troposphere and MBL is 1.5 ppm in summer, the potential errors in estimated regional GPP by the presented methods could be less than 5–10% from substituting the MBL reference.

[37] It is therefore also paramount that the ecosystem model used to derive the flux field for footprint integration is validated at some locations within and near the footprint area. Our confidence in both the concentration-derived and footprint-integrated regional GPP estimates is gained from the fact that the BEPS model used for GPP mapping agreed well with EC-derived GPP at a given site within the flux footprint. This eases our concern about possible significant model biases. The comparisons of these regional GPP estimates with EC flux measurements showed that they had similar seasonal patterns but the regional estimates were consistently smaller than local EC-derived GPP throughout the growing season in 2003. The annual differences were

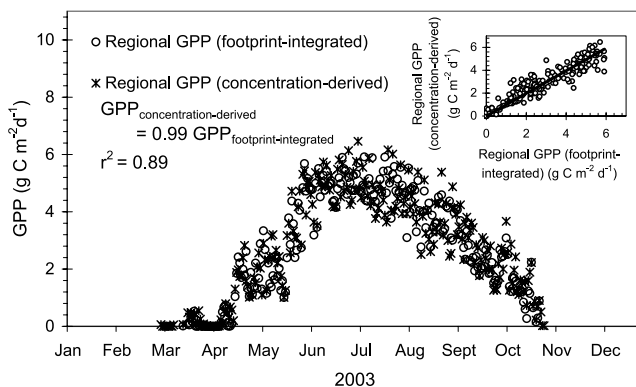


**Figure 9.** Comparison of concentration-derived regional GPP with footprint-integrated regional GPP on a daily time basis for 2003. The inset shows the linear regression between these two GPP estimates.

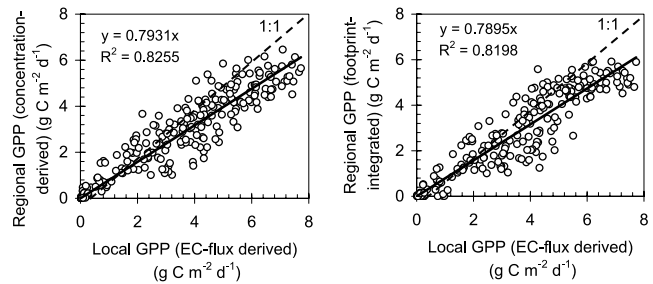


**Figure 10.** Comparisons of concentration-derived and footprint-integrated regional GPP with EC-derived local GPP on a daily time basis.

about 20–25%. The spatial representations of these two GPP estimates are very different: the EC footprint is the relatively homogeneous old black spruce while the concentration footprint is covered by boreal needle evergreen and deciduous broadleaf forests, shrub land, grass land, crop land, and lakes. The discrepancies between these two GPP estimates reflect the differences in the underlying land surface. From the GPP maps modeled by BEPS we have quantitatively evaluated that GPP values for nonforest types are much lower than that of the SOBS site, and this is consistent with the fact that both concentration-derived and concentration-footprint-integrated GPP values are considerably lower than the EC measurements. This large difference indicates the importance of considering the surface heterogeneity when we attempt to extrapolate site measurements to the region. It is encouraging to see that atmospheric  $\text{CO}_2$  concentration data can be used effectively for this upscaling purpose.

[38] There are three main assumptions made in obtaining the concentration-derived GPP during daytime [see *J. M. Chen et al.*, 2007]. In using this methodology, caution should be taken against potential errors due to (1) conditions when the PBL is not well mixed during the day, (2) highly heterogeneous atmospheric conditions such as those caused by water-land interfaces and complex terrain, and (3) diurnally variable anthropogenic  $\text{CO}_2$  sources. At nighttime, the atmosphere is highly stratified, and the similarity of uniform vertical mixing within the PBL is no longer valid. This

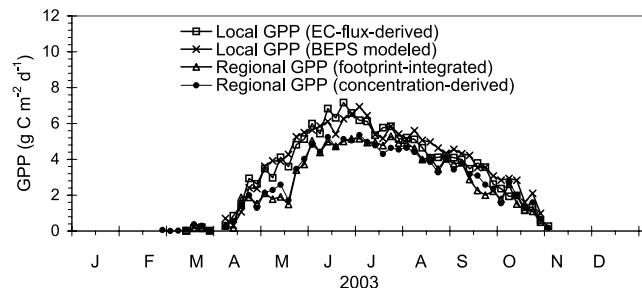


**Figure 11.** Mean 5-d GPP estimated by four different approaches based on EC flux and  $\text{CO}_2$  concentration measurements at the SOBS site, 2003.

**Table 3.** Monthly and Annual GPP Estimates From These Four Approaches for the SOBS Tower, 2003<sup>a</sup>

Scales	Methods	Mar	Apr	May	Jun	Jul	Aug	Sep	Oct	Annual
Local	EC flux derived	1.8	40.4	126.4	192.3	177.0	137.1	102.8	40.8	818.6
	BEPS modeled		30.5	138.4	179.7	180.3	150.2	110.7	56.9	846.7
Regional	Footprint integrated	1.2	26.7	77.7	145.5	155.5	127.9	76.6	38.1	649.2
	Concentration derived	3.3	27.3	86.5	145.7	149.1	120.0	86.3	46.0	664.2

<sup>a</sup>Units are  $\text{g C m}^{-2}$ .

methodology is therefore not applicable to extracting nighttime  $F_{\text{NEE}}$  or  $R$ .

[39]  $\text{CO}_2$  concentration data can be possibly used to infer  $F_{\text{NEE}}$  and  $R$  by tuning an ecosystem model when the atmospheric diffusion during daytime and nighttime is reasonably well simulated [B. Chen *et al.*, 2006a, 2006b]. It is feasible to retrieve  $R$  and  $F_{\text{NEE}}$  at regional scale by combining concentration footprint modeling with ecological modeling based on remote sensing. Simple PBL budget analysis making use of the differences in the  $\text{CO}_2$  mixing ratio between the surface layer and the free troposphere ( $C_{\text{FT}}$ ) to compute  $F_{\text{NEE}}$  on a monthly basis has been explored [Helliker *et al.*, 2004; Bakwin *et al.*, 2004; Lai *et al.*, 2006]. All of them used the marine boundary layer data to estimate  $C_{\text{FT}}$ . The  $\text{CO}_2$  entrainment at the CBL top is critical to this methodology. Helliker *et al.* [2004] estimated the vertical transfer by analyzing the budget of water vapor in the CBL with the surface flux of water vapor measured by EC methods, while the others used National Centre for Environmental Prediction (NECP) reanalysis data for the same purpose. These simple budget analyses have been shown to be successful on monthly and seasonal bases, but biases and uncertainties are still considerable [Bakwin *et al.*, 2004; Lai *et al.*, 2006; Crevoisier *et al.*, 2006]. In comparison with this methodology for net carbon exchange, our methods of deriving GPP during the daytime and  $R$  during both nighttime and daytime has the advantage of inferring carbon components necessary for model validation and ecosystem parameter optimization for regional (i.e.,  $\sim 10^5 \text{ km}^2$ ) applications.

## 6. Conclusions

[40] To quantify regional carbon fluxes using high-frequency  $\text{CO}_2$  concentration measurements, we have

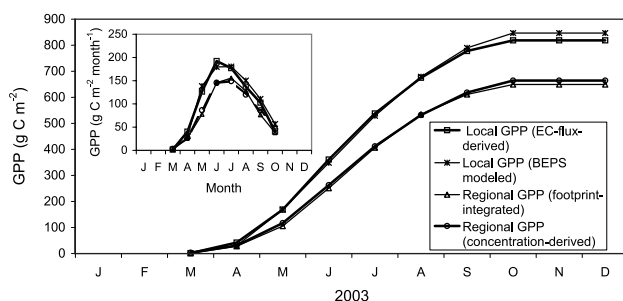


**Figure 12.** Annual cumulations of four GPP estimates for the SOBS site and the region around the site, 2003. The inset shows seasonal courses of the monthly total GPP.

explored and compared two independent methods: (1) PBL carbon budgeting using an integrated ecosystem-boundary model (i.e., BEPS-VDS), and (2) remote sensing based concentration footprint integration using a spatially explicit ecosystem model (BEPS) driven by remote sensing inputs and a new concentration footprint model (SAFE). The following three conclusions were drawn from the application of these methodologies to the SOBS tower in 2003 after the validation of BEPS using EC measurements at the site:

[41] 1. Both concentration-derived and footprint-integrated GPP values agreed well and the model used for GPP estimation within the footprint agreed well with EC measurements, suggesting that these two methods are both useful for obtaining regional carbon flux information.

[42] 2. These two methods have advantages and disadvantages: the concentration-derived GPP does not indicate the size of the source area, while the remote sensing based footprint integrating method quantifies the source area. The former is vulnerable to PBL height simulations and requires some assumptions (see section 5), while the latter is sensitive to model parameterization in both the ecosystem model (i.e., BEPS) and footprint model (SAFE). To use the two methods as a pair is a practical and effective means to derive regional carbon fluxes (i.e., GPP in this study) with high temporal resolution (i.e., at daily time steps). Combining these two methods has an obvious advantage over those approaches for net carbon flux [e.g., Helliker *et al.*, 2004; Bakwin *et al.*, 2004].

[43] 3. The influence of the inhomogeneous surface over the footprint on the atmospheric  $\text{CO}_2$  is smoothed by the CBL dynamics, and the evolution of atmospheric  $\text{CO}_2$  with time during 24 h represents the integrated influence of the surface flux at a regional scale ( $10^2$ – $10^4 \text{ km}^2$ ). This study shows that atmospheric  $\text{CO}_2$  concentration data can be used effectively to extrapolate site  $\text{CO}_2$  flux measurements to a region.

[44] **Acknowledgments.** This work is supported by the Canadian Foundation for Climate and Atmospheric Sciences as part of the Fluxnet Canada Research Network.

## References

- Arain, A., T. A. Black, A. G. Barr, P. G. Jarvis, J. M. Massheder, D. L. Verseghy, and Z. Nestic (2002), Effects of seasonal and interannual climate variability on net ecosystem productivity of boreal deciduous and conifer forests, *Can. J. For. Res.*, 32, 878–891.
- Bakwin, P. S., P. P. Tans, D. F. Hurst, and C. Zhao (1998), Measurements of carbon dioxide on very tall towers: Results of the NOAA/CMDL program, *Tellus, Ser. B*, 50, 401–415.
- Bakwin, P. S., K. J. Davis, C. Yi, S. C. Wofsy, J. W. Munger, L. Haszpra, and Z. Barcza (2004), Regional carbon dioxide fluxes from mixing ratio data, *Tellus, Ser. B*, 56, 301–311.

- Baldocchi, D. D., et al. (2001), Fluxnet: A new tool to study the temporal and spatial variability of ecosystem-scale carbon dioxide, water vapor, and energy flux densities, *Bull. Am. Meteorol. Soc.*, *82*, 2415–2434.
- Barr, A. G., T. A. Black, E. H. Hogg, N. Kljun, K. Morgenstern, and Z. Nestic (2004), Inter-annual variability in the leaf area index of a boreal aspen–hazelnut forest in relation to net ecosystem production, *Agric. For. Meteorol.*, *126*, 237–255.
- Black, T. A., G. den Hartog, H. Neumann, P. Blanken, P. Yang, Z. Nestic, S. Chen, C. Russel, P. Voroney, and R. Stabeler (1996), Annual cycles of CO<sub>2</sub> and water vapor fluxes above and within a Boreal aspen stand, *Global Change Biol.*, *2*, 219–229.
- Bousquet, P., P. Ciais, P. Peylin, M. Ramonet, and P. Monfray (1999), Inverse modeling of annual atmospheric CO<sub>2</sub> sources and sinks: 1. Method and control inversion, *J. Geophys. Res.*, *104*, 26,161–26,178.
- Chen, B., and J. M. Chen (2007), Diurnal, seasonal and inter-annual variability of carbon isotope discrimination at the canopy level in response to environmental factors in a boreal forest ecosystem, *Plant Cell Environ.*, *30*, 1223–1239.
- Chen, B., J. M. Chen, J. Liu, D. Chan, K. Higuchi, and A. Shashkov (2004), A vertical diffusion scheme to estimate the atmospheric rectifier effect, *J. Geophys. Res.*, *109*, D04306, doi:10.1029/2003JD003925.
- Chen, B., J. M. Chen, and D. Worthy (2005), Interannual variability in the atmospheric CO<sub>2</sub> rectification over a boreal forest region, *J. Geophys. Res.*, *110*, D16301, doi:10.1029/2004JD005546.
- Chen, B., J. M. Chen, P. P. Tans, and L. Huang (2006a), Modeling dynamics of stable carbon isotopic exchange between a boreal ecosystem and the atmosphere, *Global Change Biol.*, *12*, 1842–1867.
- Chen, B., J. M. Chen, L. Huang, and P. P. Tans (2006b), Simulating dynamics of  $\delta^{13}\text{C}$  of CO<sub>2</sub> in the planetary boundary layer over a boreal forest region: Covariation between surface fluxes and atmospheric mixing, *Tellus, Ser. B*, *58*, 537–549.
- Chen, B., J. M. Chen, M. Gang, C.-W. Yuen, K. Higuchi, and D. Chan (2007), Modeling and scaling coupled energy, water, and carbon fluxes based on remote sensing: An application to Canada's landmass, *J. Hydro-meteorol.*, *8*, 123–143.
- Chen, J. M., J. Liu, J. Cihlar, and M. L. Guolden (1999), Daily canopy photosynthesis model through temporal and spatial scaling for remote sensing applications, *Ecol. Modell.*, *124*, 99–119.
- Chen, J. M., et al. (2002), Validation of Canada-wide leaf area index maps using ground measurements and high and moderate resolution satellite imagery, *Remote Sens. Environ.*, *80*, 165–184.
- Chen, J. M., C. H. Menges, and S. G. Leblanc (2005), Global mapping of foliage clumping index using multi-angular satellite data, *Remote Sens. Environ.*, *97*, 447–457.
- Chen, J. M., B. Chen, K. Higuchi, J. Liu, D. Chan, D. Worthy, P. Tans, and T. A. Black (2006), Boreal ecosystems sequestered more carbon in warmer years, *Geophys. Res. Lett.*, *33*, L10803, doi:10.1029/2006GL025919.
- Chen, J. M., B. Chen, and P. Tans (2007), Deriving daily carbon fluxes from hourly CO<sub>2</sub> mixing ratios measured on the WLEF tall tower: An upscaling methodology, *J. Geophys. Res.*, *112*, G01015, doi:10.1029/2006JG000280.
- Crevoisier, C., M. Gloor, E. Gloaguen, L. W. Horowitz, J. Sarmiento, C. Sweeney, and P. Tans (2006), A direct carbon budgeting approach to infer carbon sources and sinks: Design and synthetic application to complement the NACP observation network, *Tellus, Ser. B*, *58*, 366–375.
- Enting, I. G., C. M. Trudinger, and R. J. Francey (1995), A synthesis inversion of the concentration and  $\delta^{13}\text{C}$  of atmospheric CO<sub>2</sub>, *Tellus, Ser. B*, *47*, 35–52.
- Fan, S., M. Gloor, J. Mahlman, S. Pacala, J. Sarmiento, T. Takahashi, and P. Hans (1998), A large terrestrial carbon sink in North America implied by atmospheric and oceanic carbon dioxide data and models, *Science*, *282*, 442–446.
- Friedlingstein, P., J. L. Dufresne, P. M. Cox, and P. Rayner (2003), How positive is the feedback between climate change and the carbon cycle?, *Tellus, Ser. B*, *55*, 692–700.
- Fung, I. Y., K. Prentice, E. Matthews, J. Lerner, and G. Russell (1983), Three-dimensional tracer model study of atmospheric CO<sub>2</sub>: Response to seasonal exchanges with the terrestrial biosphere, *J. Geophys. Res.*, *88*, 1281–1294.
- Fung, I. Y., S. C. Doney, K. Lindsay, and J. John (2005), Evolution of carbon sinks in a changing climate, *Proc. Nat. Acad. Sci.*, *102*, 11,201–11,206.
- Gerbig, C., J. C. Lin, S. C. Wofsy, B. C. Daube, A. E. Andrews, B. B. Stephens, P. S. Bakwin, and C. A. Grainger (2003), Toward constraining regional-scale fluxes of CO<sub>2</sub> with atmospheric observations over a continent: 1. Observed spatial variability from airborne platforms, *J. Geophys. Res.*, *108*(D24), 4756, doi:10.1029/2002JD003018.
- GLOBALVIEW-CO<sub>2</sub> (2005), *Cooperative Atmospheric Data Integration Project: Carbon Dioxide* [CD-ROM], NOAA Clim. Monit. and Diag. Lab., Boulder, Colo. (Available via anonymous FTP to ftp.cmdl.noaa.gov, Path: ccg/co2/GLOBALVIEW)
- Gloor, M., S. M. Fan, S. Pacala, J. Sarmiento, and M. Ramonet (1999), A model-based evaluation of inversions of atmospheric transport, using annual mean mixing ratios, as a tool to monitor fluxes of nonreactive trace substances like CO<sub>2</sub> on a continental scale, *J. Geophys. Res.*, *104*, 14,245–14,260.
- Gloor, M., P. Bakwin, D. Hurst, L. Lock, R. Draxler, and P. Tans (2001), What is the concentration footprint of a tall tower?, *J. Geophys. Res.*, *106*, 17,831–17,840.
- Griffis, T. J., T. A. Black, K. Morgenstern, A. G. Barr, Z. Nestic, G. B. Drewitt, and D. Gaumont-Guay (2003), Ecophysiological controls on the carbon balances of three southern boreal forests, *Agric. For. Meteorol.*, *125*, 207–223.
- Gurney, K. R., et al. (2002), Towards robust regional estimates of CO<sub>2</sub> sources and sinks using atmospheric transport models, *Nature*, *415*, 626–630.
- Helliker, B. R., J. A. Berry, A. K. Betts, P. S. Bakwin, K. J. Davis, A. S. Denning, J. R. Ehleringer, J. B. Miller, M. P. Butler, and D. M. Ricciuto (2004), Estimates of net CO<sub>2</sub> flux by application of equilibrium boundary layer concepts to CO<sub>2</sub> and water vapor measurements from a tall tower, *J. Geophys. Res.*, *109*, D20106, doi:10.1029/2004JD004532.
- Horst, T. W., and J. C. Weil (1992), Footprint estimation for scalar flux measurements in the atmospheric surface layer, *Boundary Layer Meteorol.*, *59*, 279–296.
- Jarvis, P. G., J. M. Massheder, S. E. Hale, J. B. Moncrieff, M. Rayment, and S. L. Scott (1997), Seasonal variation of carbon dioxide, water and energy exchanges of a boreal black spruce forest, *J. Geophys. Res.*, *102*, 28,953–28,966.
- Ju, W., J. M. Chen, T. A. Black, A. Barr, J. Liu, and B. Chen (2006), Modeling coupled water and carbon fluxes in a boreal aspen forest, *Agric. For. Meteorol.*, *140*, 136–151.
- Kljun, N., R. Kormann, M. W. Rotach, and F. X. Meixner (2003), Comparison of the Lagrangian footprint model LPDM-B with an analytical footprint model, *Boundary Layer Meteorol.*, *106*, 349–355.
- Kljun, N., T. A. Black, T. J. Griffis, A. G. Barr, D. Gaumont-Guay, K. Morgenstern, J. H. McCaughey, and Z. Nestic (2006), Response of net ecosystem productivity of three boreal forest stands to drought, *Ecosystems*, *9*, 1128–1144.
- Lacelle, B. (1997), Canada's soil organic carbon database, in *Soil Processes and the Carbon Cycle*, edited by R. Lal et al., pp. 93–102, CRC Press, New York.
- Lai, C.-T., A. J. Schauer, C. Owensby, J. M. Ham, B. Helliker, P. Tans, and J. R. Ehleringer (2006), Regional CO<sub>2</sub> fluxes inferred from mixing ratio measurements: estimates from flask air samples in central Kansas, USA, *Tellus, Ser. B*, *58*, 523–536.
- Law, B. E., et al. (2002), Environmental controls over carbon dioxide and water vapor exchange of terrestrial vegetation, *Agric. For. Meteorol.*, *113*, 97–120, doi:10.1016/S0168-1923(02)00104-1.
- Levy, P. E., A. Grelle, A. Lindroth, M. Mölder, P. G. Jarvis, B. Kruijt, and J. B. Moncrieff (1999), Regional-scale CO<sub>2</sub> fluxes over central Sweden by a boundary layer budget method, *Agric. For. Meteorol.*, *98/99*, 169–180.
- Lin, J. C., C. Gerbig, S. C. Wofsy, A. E. Andrews, B. C. Daube, C. A. Grainger, B. B. Stephens, P. S. Bakwin, and D. Y. Hollinger (2004), Measuring fluxes of trace gases at regional scales by Lagrangian observations: Application to the CO<sub>2</sub> Budget and Rectification Airborne (COBRA) study, *J. Geophys. Res.*, *109*, D15304, doi:10.1029/2004JD004754.
- Lin, J. C., C. Gerbig, S. C. Wofsy, B. C. Daube, D. M. Matross, V. Y. Chow, E. Gottlieb, A. E. Andrews, M. Pathmathevan, and J. W. Munger (2006), What have we learned from intensive atmospheric sampling field programs of CO<sub>2</sub>?, *Tellus, Ser. B*, *58*, 331–343.
- Liu, J., J. M. Chen, J. Cihlar, and W. Chen (1999), Net primary productivity distribution in BOREAS region from a process model using satellite and surface data, *J. Geophys. Res.*, *104*, 27,735–27,754.
- Liu, J., J. M. Chen, J. Cihlar, and W. Chen (2002), Net primary productivity mapped for Canada at 1-km resolution, *Global Ecol. Biogeogr.*, *11*, 115–129.
- Masarie, K. A., and P. P. Tans (1995), Extension and integration of atmospheric carbon dioxide data into a globally consistent measurement record, *J. Geophys. Res.*, *100*, 593–1610.
- Matross, D., A. Andrews, and M. Pathmathevan (2006), Estimating regional carbon exchange in New England and Quebec by combining atmospheric, ground-based and satellite data, *Tellus, Ser. B*, *58*, 344–358.
- Moeng, C. H., and J. C. Wyngaard (1989), Evaluation of turbulent transport and dissipation closures in 2nd-order modeling, *J. Atmos. Sci.*, *46*, 2311–2330.

- Pasquill, F. (1974), *Atmospheric Diffusion*, 2nd ed., 437 pp., J. Wiley, New York.
- Potosnak, M. J., S. C. Wofsy, A. S. Denning, T. J. Conway, J. W. Munger, and D. H. Barnes (1999), Influence of biotic exchange and combustion sources on atmospheric CO<sub>2</sub> concentration in New England from observations at a forest flux tower, *J. Geophys. Res.*, *104*, 9561–9569.
- Raupach, M. R., O. T. Denmead, and F. X. Dunin (1992), Challenges in linking atmospheric CO<sub>2</sub> concentrations to fluxes at local and regional scales, *Aust. J. Bot.*, *40*, 697–716.
- Rodenbeck, C., S. Houweling, M. Gloor, and M. Heimann (2003), CO<sub>2</sub> flux history 1982–2001 inferred from atmospheric data using a global inversion of atmospheric transport, *Atmos. Chem. Phys.*, *3*, 1919–1964.
- Schmid, H. P. (1994), Source areas for scalar and scalar fluxes, *Boundary Layer Meteorol.*, *67*, 293–318.
- Schut, P., J. Shields, C. Tarnocai, D. Coote, and I. Marshall (1994), Soil landscapes of Canada: An environmental reporting tool, paper presented at Canadian Conference on GIS, Agriculture Canada, Ottawa, Canada, 6–10 June.
- Sellers, P. J., et al. (1997), BOREAS in 1997: Experiment overview, scientific results, and future directions, *J. Geophys. Res.*, *102*, 28,731–28,769.
- Shields, J. A., C. Tarnocai, K. W. G. Valentine, and K. B. MacDonald (1991), *Soil Landscapes of Canada: Procedures Manual and User's Hand Book, Agric. Can. Publ. 1868/E*, Agric. Can., Ottawa, Canada.
- Styles, J. M., J. Lloyd, D. Zolotoukhine, K. A. Lawton, N. Tchebakova, R. J. Francey, A. Arneeth, D. Salamakho, O. Kolle, and E.-D. Schulze (2002), Estimates of regional surface carbon dioxide exchange and carbon and oxygen isotope discrimination during photosynthesis from concentration profiles in the atmospheric boundary layer, *Tellus, Ser. B*, *54*, 768–783.
- Tans, P. P., I. Y. Fung, and T. Takahashi (1990), Observational constraints on the global atmospheric CO<sub>2</sub> budget, *Science*, *247*, 1431–1438.
- van Ulden, A. P. (1978), Simple estimates for vertical diffusion from sources near the ground, *Atmos. Environ.*, *12*, 2125–2129.
- Wyngaard, J. C., and R. A. Brost (1984), Top-down and bottom-up diffusion of a scalar in the convective boundary layer, *J. Atmos. Sci.*, *41*, 102–112.
- Zhang, D., and R. Anthes (1982), A high-resolution model of the planetary boundary layer-sensitivity tests and comparisons with SESAME-79 data, *J. Appl. Meteorol.*, *21*, 1594–1608.
- 
- T. A. Black, Biometeorology and Soil Physics Group, Faculty of Land and Food Systems, University of British Columbia, 2357 Main Mall, Vancouver, BC, V6T 1Z4, Canada.
- B. Chen, J. M. Chen, and G. Mo, Department of Geography and Program in Planning, University of Toronto, Toronto, ON, M5S 3G3, Canada. (baozhang.chen@ubc.ca)
- D. E. J. Worthy, Air Quality Research Branch, Meteorological Service of Canada, 4905 Dufferin Street, Toronto, Ontario, M3H 5T4 Canada.